

# The moment duration scaling relation for slow rupture arises from transient rupture speeds

Kjetil Thøgersen<sup>1,2\*</sup>, Henrik Andersen Sveinsson<sup>1,3</sup>, Julien Scheibert<sup>4</sup>, François Renard<sup>1,2,5</sup>, Anders Malthe-Sørensen<sup>1,3</sup>

<sup>1</sup>Physics of Geological Processes, The NJORD Centre, University of Oslo, Norway

<sup>2</sup>Department of Geosciences, University of Oslo, Norway

<sup>3</sup>Department of Physics, University of Oslo, Norway

<sup>4</sup>Univ Lyon, Ecole Centrale de Lyon, ENISE, ENTPE, CNRS, Laboratoire de Tribologie et Dynamique des Systèmes LTDS, F-69134, Ecully, France

<sup>5</sup>University Grenoble Alpes, University Savoie Mont Blanc, CNRS, IRD, IFSTTAR, ISTERre, 38000 Grenoble, France

## Key Points:

- A Burridge-Knopoff model with only two dimensionless parameters; the homogeneous stress on a fault and a velocity strengthening friction term.
- The simplicity of the model allows for both numerical and analytical calculations of moment versus duration scaling relationships during fault slip.
- Moment versus duration scaling relation for slow events arises from transient rupture speeds.

## Plain language summary

Observations have shown that the duration of earthquakes is related to the seismic moment through a power law. The power law exponent is different for regular earthquakes and slow aseismic rupture, and the origin of this difference is currently debated in the literature. In this letter, we introduce a minimal mechanical friction model that contains both slow and regular earthquakes, and demonstrate that the different power laws emerge naturally within the model because the propagation speed of slow earthquakes decays as a power law in time whereas the propagation speed of regular earthquakes remains fairly constant.

---

\*kjetil.thogersen@fys.uio.no

**Abstract**

28 The relation between seismic moment and earthquake duration for slow rupture fol-  
 29 lows a different power law exponent than sub-shear rupture. The origin of this dif-  
 30 ference in exponents remains unclear. Here, we introduce a minimal one-dimensional  
 31 Burridge-Knopoff model which contains slow, sub-shear and super-shear rupture, and  
 32 demonstrate that different power law exponents occur because the rupture speed of  
 33 slow events contains long-lived transients. Our findings suggest that there exists a  
 34 continuum of slip modes between the slow and fast slip end-members, but that the  
 35 natural selection of stress on faults can cause less frequent events in the intermediate  
 36 range. We find that slow events on one-dimensional faults follow  $\bar{M}_{0,\text{slow},1D} \propto \bar{T}^{0.63}$   
 37 with transition to  $\bar{M}_{0,\text{slow},1D} \propto \bar{T}^{\frac{3}{2}}$  for longer systems or larger prestress, while the  
 38 sub-shear events follow  $\bar{M}_{0,\text{sub-shear},1D} \propto \bar{T}^2$ . The model also predicts a super-shear  
 39 scaling relation  $\bar{M}_{0,\text{super-shear},1D} \propto \bar{T}^3$ . Under the assumption of radial symmetry, the  
 40 generalization to two-dimensional fault planes compares well with observations.  
 41

## 1 Introduction

Over the last decades, an increasing number of slow slip events on faults have been reported (Bürgmann, 2018). A measure that is viewed as a key to unravelling the mechanism of slow and fast rupture is the relation between seismic moment  $M_0$  and slip event duration  $T$ . Regular fast earthquakes have long been known to follow a moment duration scaling relation of  $M_0 \propto T^3$ . Ide et al. suggested that slow events follow a unified scaling relation  $M_0 \propto T$  (Ide, Beroza, Shelly, & Uchide, 2007). They suggested that the linear relation between moment and duration for slow events can be explained in two ways: (1) the average slip is proportional to the fault length as for fast propagation, and the stress drop is constant for all events, which gives the relation  $M_0 \propto T$ . (2) the slip amount is constant for all events, and the fault area increases linearly with time  $L^2 \propto T$ , which results in  $M_0 \propto T$ . Peng and Gomberg (2010) elaborated on the ideas of Ide et al. (2007) and reached a different conclusion; that rupture should span a continuum between fast and slow velocity end-members. Later studies have reported on a variety of scalings between moment and duration ranging from  $M_0 \propto T$  to  $M_0 \propto T^2$  (Aguiar, Melbourne, & Scrivner, 2009; Frank, Rousset, Lasserre, & Campillo, 2018; Gao, Schmidt, & Weldon, 2012; Ide, Imanishi, Yoshida, Beroza, & Shelly, 2008).

The shape of slip patches can also influence the observed scaling. Ben-Zion (2012) argued that fractal slip patches can result in a scaling relation  $M_0 \propto T^2/\log(T)$  because the average displacement is approximately constant rather than proportional to the rupture dimension. Bounded propagation can also play an important role (Ben-Zion, 2012; Gomberg, Wech, Creager, Obara, & Agnew, 2016). Gomberg et al. (2016) suggested that the scaling relation between moment and duration is the same for slow and fast events, but that a transition occurs between a two-dimensional scaling and a one-dimensional scaling when the rupture propagation switches from unbounded to bounded in one direction. Assuming the fault displacement can be approximated using dislocation theory, this results in a transition from  $T^2$  to  $T$ . They suggest that there should be a bimodal but continuous distribution of slip modes, and that a difference in scaling relations alone does not imply a fundamental difference between fast and slow slip. The above mentioned theoretical considerations implicitly assume constant rupture velocity. However, this contradicts observations by Gao et al. (2012) that show that the average rupture speed for slow events decreases with increasing seismic moment, which is a strong indication of transient rupture speeds.

Slow slip events emerge in numerical models with rate-and-state friction. Colella, Dieterich, and Richards-Dinger (2011) simulated a Cascadia-like subduction zone using rate-and-state friction. They analyzed a large number of slip events, and found that the seismic moment  $M_w$  scales as  $M_w \propto T^{1.5}$  for  $M_w \leq 5.6$  with a transition to  $M_w \propto T^2$  for  $M_w > 5.6$ . Shibasaki, Obara, Matsuzawa, and Hirose (2012) modeled the subduction zone of southwest Japan with rate-and-state friction. For slow events, they found a scaling  $M_0 \propto T^{1.3}$ . Liu (2014) used rate-and-state friction on a 3D subduction fault model and found a scaling  $M_0 \propto T^{1.85}$ . Romanet, Bhat, Jolivet, and Madariaga (2018) highlighted the role of interactions between faults. They argue that the scaling relationships of slow slip events and earthquakes emerge from geometrical complexities due to interactions between fault segments. The moment duration scalings have not only been addressed using rate-and-state friction. Ide (2008) introduced a brownian walk model for slow rupture, where the assumption is that there is a random expansion and contraction of the fault area, so that its radius can be described as a Brownian walk with a damping term. This model predicts  $M_0 \propto T$  for large  $T$ .

Here, our goal is to answer the following two questions: (1) Is there a separation of two distinct classes (Ide et al., 2007), or is there a continuum of possible scaling relations between the fast and slow end-members (Peng & Gomberg, 2010)? (2) Can a difference in  $M_0 - T$  scaling relations alone be attributed to different physical mecha-

nisms behind slow and fast rupture? We address both (1) and (2) through a Burridge-Knopoff type model with Amontons-Coulomb friction with a velocity strengthening friction term that has previously been shown to contain a large variety of rupture phenomena, including sub-shear, super-shear and slow propagation (Thøgersen et al., 2019). Velocity strengthening friction has been shown to be a generic feature of dry friction (Bar-Sinai, Spatschek, Brener, & Bouchbinder, 2014), and has been reported in Halite shear zones at low slip speeds or large confining pressures (Shimamoto, 1986). The friction law can also be interpreted as a transition from a dry contact to a lubricated sliding regime with increasing velocity (a Stribeck curve) under the additional assumption that the transition from dry to contact to lubricated sliding occurs at a small sliding speed (Gelinck & Schipper, 2000; Olsson, Åström, De Wit, Gäfvert, & Lischinsky, 1998).

For homogeneously stressed faults, the model can be reduced to only two dimensionless parameters  $\bar{\tau}$  and  $\bar{\alpha}$  representing the prestress and a velocity strengthening friction term, respectively. The advantage of such approach is that the simplicity of the model allows us to calculate moment duration scaling relations both through numerical simulations and through analytical calculations. Through numerical simulations, we demonstrate that there exists a continuum of rupture modes between the slow and fast end-members, but that the most likely selection of  $\bar{\tau}$  in nature produces two distinct classes separating sub-shear and slow rupture velocities. Through analytical calculations, we show that the scaling relation for slow fronts arises due to long-lived transients in the rupture velocity. Such transient rupture velocity has been observed in nature through a dependence on the average rupture speed on the seismic moment for slow fronts (Gao et al., 2012). In addition, the model predicts a separate scaling for super-shear rupture not previously reported in the literature.

## 2 A one-dimensional Burridge-Knopoff containing slow and fast rupture

We solve the one-dimensional Burridge-Knopoff model (Burridge & Knopoff, 1967) with Amontons-Coulomb friction with a linear velocity strengthening term. The dimensionless equation of motion for a chain of  $N$  blocks can be written as (a detailed derivation can be found in the supplementary information)

$$\ddot{\bar{u}}_i - \bar{u}_{i-1} - \bar{u}_{i+1} + 2\bar{u}_i + \bar{\alpha}\dot{\bar{u}}_i - \bar{\tau}^\pm = 0, \quad \forall i \in [0, N], \quad (1)$$

where  $\bar{u}$  is the dimensionless displacement

$$\bar{\tau}^\pm = \frac{\tau/\sigma_N \mp \mu_k}{\mu_s - \mu_k} \quad (2)$$

is the dimensionless prestress where  $\sigma_N$  is the normal stress,  $\tau$  is the initial shear stress, and  $\mu_s$  and  $\mu_k$  are the static and dynamic coefficients of friction, respectively.  $\pm$  denotes the sign of the block velocity. For positive velocities, we only need to consider  $\bar{\tau}^+$ , but negative velocities can occur in a small subset of our simulations. In such situations, we need to prescribe the relation between  $\mu_s$  and  $\mu_k$ , which we set to  $\mu_s = 2\mu_k$ , so that  $\bar{\tau}^- = \bar{\tau}^+ + 2$ . In the rest of the paper we will use  $\bar{\tau}$  as a reference to  $\bar{\tau}^+$ . The second dimensionless parameter

$$\bar{\alpha} = \frac{\alpha}{\sqrt{\rho E}} \quad (3)$$

is a viscous term, where  $\rho$  is the density,  $E$  is the elastic modulus, and  $\alpha$  is a velocity strengthening term with units [Pa s/m].  $\bar{\alpha}$  can range from 0 to infinity, where  $\bar{\alpha} = 0$  recovers the ordinary Amontons-Coulomb friction without viscosity.  $\bar{\tau}$  has an upper limit of 1, where the prestress equals the static friction threshold. For  $\bar{\tau} < 0$ , steady state propagation does not occur (Amundsen et al., 2015). This corresponds to a prestress

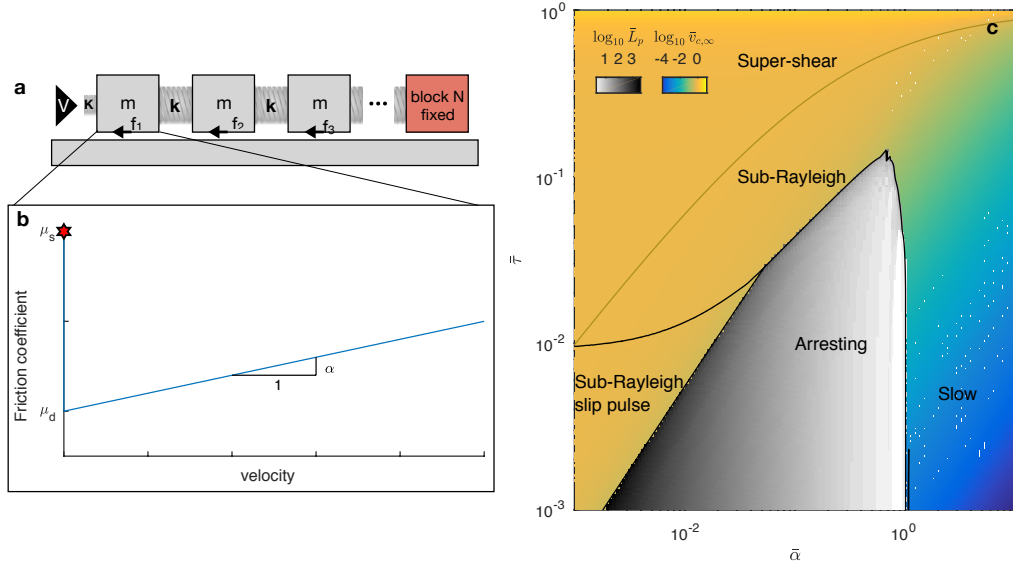


**Figure 1.** (a) We solve the one-dimensional Burridge-Knopoff model with Amontons-Coulomb friction with velocity-strengthening dynamic friction for homogeneously loaded faults.  $V$  is the driving velocity,  $K$  is the driving spring constant,  $m$  is the block mass,  $k$  is the spring constant, and  $f_i$  is the friction force on block  $i$ . The friction law is given by a static friction coefficient  $\mu_s$ , and a dynamic friction coefficient  $\mu_d$  plus a velocity strengthening term  $\alpha v$  (b). To obtain the seismic moment and duration for a given fault length we fix the block at position  $N$ . The model can be written in dimensionless units with only two parameters:  $\bar{\tau}$  representing the prestress on the fault, and  $\bar{\alpha}$  representing the velocity strengthening friction term. This simple model produces a large variety of slip, including, slip pulses, cracks, sub-Rayleigh rupture, super-shear rupture, slow rupture, and arresting fronts (c). The colorbars show the rupture length  $\bar{L}$  of arresting fronts, and the steady state rupture speed  $\bar{v}_{c,\infty}$  for given  $\bar{\tau}$  and  $\bar{\alpha}$  (adapted from Thøgersen et al. (2019))

139 below the dynamic friction level. We thus simulate  $\bar{\tau} \in [10^{-7}, 1]$  and  $\bar{\alpha} \in [10^{-3}, 10]$ .  
 140 The boundary conditions assuming triggering through soft tangential loading (small  
 141 driving velocity  $V$  and driving spring stiffness  $K$ ) are given by  $\bar{u}_{-1} = \bar{u}_0 + 1 - \bar{\tau}$ . The  
 142 rightmost block is fixed so that  $\bar{u}_N = 0$ . Blocks start to move once the static friction  
 143 threshold is reached, which in dimensionless units can be written as

$$\bar{u}_{i-1} + \bar{u}_{i+1} - 2\bar{u}_i \geq 1 - \bar{\tau} \quad (4)$$

144 Moving blocks restick if the velocity changes sign. The system is sketched in Figure 1a.  
 145 This model has previously been used to determine the steady state rupture velocity  
 146 which includes sub-shear, supershear, and slow rupture, as well as an arresting region  
 147 at low  $\bar{\tau}$  and intermediate  $\bar{\alpha}$  (Thøgersen et al., 2019). The steady state front speed  
 148  $\bar{v}_{c,\infty}$  can be found exactly when  $\bar{\alpha} = 0$  (Amundsen et al., 2015). For  $\bar{\alpha} > 0$  we can use  
 149 the empirical expression (Thøgersen et al., 2019)

$$\bar{v}_{c,\infty} \approx \frac{1 - e^{-\frac{\bar{\tau}}{\bar{\alpha}(1-\bar{\tau})}}}{\sqrt{1 - \bar{\tau}^2}}. \quad (5)$$

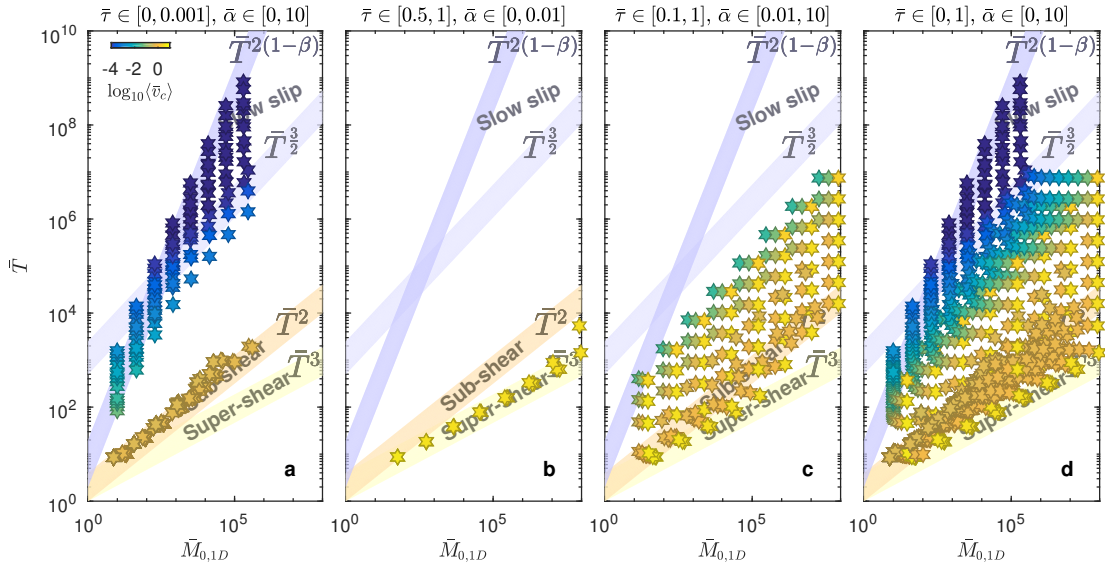


**Figure 2.** One-dimensional seismic moment  $\bar{M}_{0,1D}$  and event duration  $\bar{T}$  obtained from simulations. The color of the markers show the average front speed  $\langle \bar{v}_c \rangle$ . The origin of the four different scaling exponents  $\{2(1 - \beta), \frac{3}{2}, 2, 3\}$  is discussed in detail in the text. (a) In the limit of small  $\bar{\tau}$ , there is a separation in two distinct scalings for fast and slow events. (b) For large  $\bar{\tau}$  the model predicts super-shear rupture, which has a different scaling exponent than regular sub-shear earthquakes. (c): For intermediate  $\bar{\tau}$ , the central part of the diagram is populated. (d) Results from the entire range of  $\bar{\tau}$  and  $\bar{\alpha}$  show that moment duration can exhibit a continuum of slip modes in between the slow and fast end-members.

### 3 Moment duration scaling relations

#### 3.1 Model results

We run simulations until all blocks have ruptured or all blocks have stopped. We have performed 1120 simulations to obtain the moment duration diagram with  $N \in 5 \times 2^{\{0,7\}}$ . In dimensionless units the zeroth order moment for rupture propagation along a line is

$$\bar{M}_{0,1D} = \langle \bar{u} \rangle \bar{L}, \quad (6)$$

where  $\langle \bar{u} \rangle$  is the average displacement on a fault of length  $\bar{L}$ . We run the simulations until all blocks are immobile, or until the average velocity reaches 0.1% of the steady state slip speed  $\bar{\tau}/\bar{\alpha}$  (Thøgersen et al., 2019). The seismic moment and the duration are measured when 99% of the total displacement has been reached.

Figure 2 shows the measured  $\bar{M}_{0,1D}$  and event duration  $\bar{T}$  for all simulations. If the stress drop is small compared to the absolute shear stress, as is often found for faults (Shearer, Prieto, & Hauksson, 2006),  $\tau$  should often lie close to the dynamic level, which corresponds to  $\bar{\tau} \simeq 0$ . For low values of  $\bar{\tau}$ , the arresting region in  $(\bar{\tau}, \bar{\alpha})$  gives rise to a separation of these scaling relations, so that fast and slow rupture fall into two distinct lines in the moment duration diagram (Figure 2a). This is in line with the ideas of Ide et al. (2007). This separation occurs because steady state propagation at small  $\bar{\tau}$  and intermediate  $\bar{\alpha}$  is forbidden (Figure 1a). If we include also larger prestress values we obtain a continuum of slip modes in the moment duration diagram (Figure 2d), in line with the suggestions of Peng and Gomberg (2010). The model also predicts a second scaling relations for super-shear rupture, which is found at large  $\bar{\tau}$ , that has not previously been reported (Figure 2b).

#### 3.2 Origin of scaling relations - analytical calculations

The simplicity of the model allows an analytical treatment of several aspects which helps explain the various scaling relations between seismic moment and event duration. We summarize the analytical predictions for slip, front speed and event duration, and explain why the different scaling relations appear. A detailed derivation is given in the supplementary information.

First, we can determine the average slip on a fault. If the stress is at the dynamic level after rupture (the stress drop equals  $\bar{\tau}$ ), we can calculate  $\langle \bar{u} \rangle$  exactly

$$\langle \bar{u} \rangle = \frac{\bar{\tau} \bar{L}^2}{3} + \frac{(1 - \bar{\tau}) \bar{L}}{2}. \quad (7)$$

Equation 7 is derived for soft tangential loading, and we stress that a different boundary conditions could lead to different dependencies between  $\bar{L}$ ,  $\langle \bar{u} \rangle$  and  $\bar{\tau}$ . Combining equation 7 with equation 6 we find that the seismic moment can be written as

$$\bar{M}_{0,1D} = \frac{\bar{\tau} \bar{L}^3}{3} + \frac{(1 - \bar{\tau}) \bar{L}^2}{2}, \quad (8)$$

which only depends on the prestress  $\bar{\tau}$  and the length of the fault  $\bar{L}$ . To obtain the moment duration scaling relation we need to determine  $\bar{L}(\bar{T})$ , and thus have to combine equation 8 with information about the rupture propagation and the afterslip (i.e. the amount of slip after the propagation has stopped).

A key observation on the rupture propagation is shown in Figure 3. While fast fronts exhibit short transients and quickly reach the steady state propagation speed given by equation 5, slow rupture contains long transients where the propagation speed decays. In the figure, we have illustrated this effect as a decay in the average rupture speed  $\langle \bar{v}_c \rangle$  with increasing seismic moment  $\bar{M}_0$ . This result is in line with observations by Gao et al. (2012).

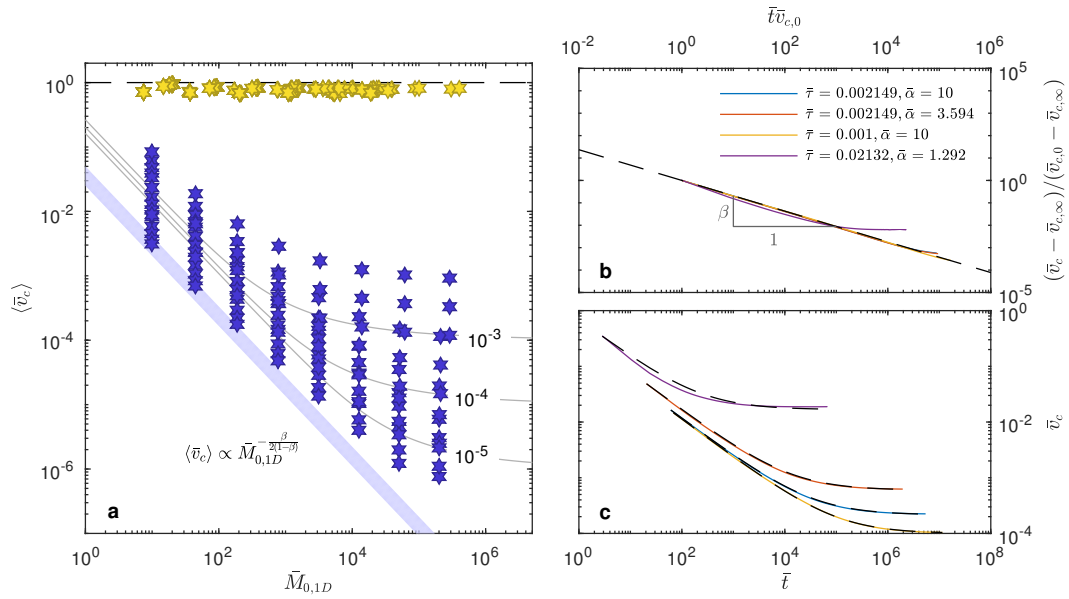


**Figure 3.** (a) Average propagation speed  $\langle \bar{v}_c \rangle$  as a function of seismic moment for  $\bar{\tau} \in [10^{-7}, 10^{-3}]$  and  $\bar{\alpha} \in [10^{-3}, 10]$ . Yellow markers show fast fronts while blue show slow fronts. Grey lines show predictions for  $\bar{\alpha} = 10$  and  $\bar{\tau} \in [10^{-5}, 10^{-3}]$  from equation 14. The prediction for  $\bar{\tau} = 0$  follows  $\langle \bar{v}_c \rangle \propto \bar{M}_{0,1D}^{-\frac{\beta}{2(1-\beta)}}$ . (b) This transient velocity can be approximated by subtracting the steady state front velocity  $v_{c,\infty}$  from equation 5 and scaling with the initial rupture velocity  $v_{c,0}$  found from equation S32. The dashed line shows  $(\bar{t}\bar{v}_{c,0})^{-\beta}$  with  $\beta = 0.6852$ . (c) The same fit when the steady state is not subtracted.



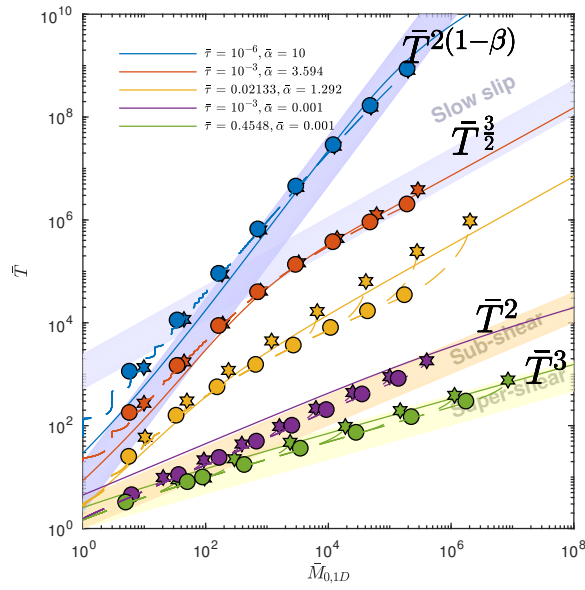


**Figure 4.** Moment duration scaling examples. Dashed lines show the evolution in time of the seismic moment. (star) shows the final value of the duration and the moment, while (circle) marks the point when the front reaches the end of the fault (i.e without afterslip) for  $N = 5 \times 2^{\{0,7\}}$ . The solid lines show the predictions of moment versus duration discussed in the text. The top three curves use the slow scaling (equation 17 and 18), while the bottom two use the fast scaling relation (equation 11). The colored regions highlight the different scaling exponents discussed in the text.

### 3.2.1 Fast regime

The short transients in the fast regime indicate that we can approximate the rupture length by

$$\bar{L} = \int_0^{\bar{t}_{\text{rupture}}} \bar{v}_c(t') dt' \approx \bar{v}_{c,\infty} \bar{t}_{\text{rupture}}, \quad (9)$$

where  $t_{\text{rupture}}$  is the time it takes for a rupture front to reach the end of the fault. The time it takes to arrest completely depends upon the existence of a backward propagating arresting front. If we assume that this backward propagation occurs at roughly the same speed as the forward propagation we obtain

$$\bar{T} \approx \frac{2\bar{L}}{\bar{v}_{c,\infty}} \quad (10)$$

so that

$$\bar{M}_{0,1D} \approx \frac{\bar{\tau}}{3} \left( \frac{\bar{v}_{c,\infty} \bar{T}}{2} \right)^3 + \frac{1-\bar{\tau}}{2} \left( \frac{\bar{v}_{c,\infty} \bar{T}}{2} \right)^2. \quad (11)$$

This relation implies that there is a separate scaling for sub-shear ( $\bar{\tau} \rightarrow 0$ ) and super-shear rupture ( $\bar{\tau} \rightarrow 1$ ) in our simulations:

$$\bar{M}_{0,\text{sub-shear},1D} \propto \bar{T}^2 \quad (12)$$

and

$$\bar{M}_{0,\text{super-shear},1D} \propto \bar{T}^3. \quad (13)$$

Note that we also predict that  $\bar{M}_{0,\text{sub-shear},1D}$  will transition to a  $\bar{T}^3$  scaling for large  $\bar{L}$  if  $\bar{\tau}$  is small but nonzero. The moment duration, in the fast regime using equation 11, is shown in the two bottom lines of Figure 4. This figure also shows numerically obtained values for the moment duration. The agreement between the numerical simulations and equation 11 is good.

### 3.2.2 Slow regime

For slow fronts,  $\bar{v}_c(\bar{t})$  is transient. To obtain an approximation for  $\bar{v}_c(\bar{t}, \bar{\alpha}, \bar{\tau})$ , we plot  $\bar{v}_c(\bar{t})$  for a selection of  $\bar{\tau}$  and  $\bar{\alpha}$  in Figure 3. All curves collapse when we subtract the steady state front velocity  $v_{c,\infty}$  and scale with the initial rupture velocity  $v_{c,0}$  given in equation S32. We can then write down

$$\bar{v}_{c,\text{slow}} \approx (\bar{v}_{c,0} - \bar{v}_{c,\infty}) (\bar{v}_{c,0} \bar{t})^{-\beta} + \bar{v}_{c,\infty} \quad (14)$$

Figure 3 shows that this relation fits well with simulations for small  $\bar{\tau}$ , and we measure empirically the exponent  $\beta \approx 0.6852$ . To obtain a parametric equation for  $\bar{M}_0$  and  $\bar{T}$ , we need to find  $\bar{T}(\bar{L})$ .  $\bar{T}$  has two main components; the time it takes to rupture a fault of length  $\bar{L}$ ,  $\bar{t}_{\text{rupture}}$ , and the time it takes for all motion to stop. Unlike for fast fronts, the arresting phase in the slow regime is not governed by a backward propagating arresting front, but rather a slow exponential decay in velocity. We denote this time  $\bar{t}_{\text{afterslip}}$ , and define

$$\bar{T} = \bar{t}_{\text{rupture}} + \bar{t}_{\text{afterslip}}. \quad (15)$$

$\bar{t}_{\text{rupture}}$  can be found from equation 14

$$\bar{L} = \int_0^{\bar{t}_{\text{rupture}}} \bar{v}_c(\bar{t}') d\bar{t}' \quad (16)$$

$$= \frac{(\bar{v}_{c,0} - \bar{v}_{c,\infty})}{(1-\beta)\bar{v}_{c,0}^\beta} \bar{t}_{\text{rupture}}^{1-\beta} + \bar{v}_{c,\infty} \bar{t}_{\text{rupture}}, \quad (17)$$

The afterslip time can also be found analytically, and the detailed calculation is given in the supplementary information. The result is

$$\bar{t}_{\text{afterslip}} = \log(100) \frac{2\bar{L}^2 \bar{\alpha}}{\pi^2} \quad (18)$$

224 where  $\log(100)$  indicates that we take the time when 99% of the slip has been ac-  
 225 cumulated (which is necessary because the afterslip is exponentially decaying). The  
 226 prediction of seismic moment versus duration can then be found using equation 8 for  
 227 the seismic moment, equation 17 for  $\bar{t}_{\text{rupture}}$  (this has to be solved numerically for  
 228 nonzero  $\bar{\tau}$ ), and equation 18 for  $\bar{t}_{\text{afterslip}}$ , with  $\bar{T} = \bar{t}_{\text{rupture}} + \bar{t}_{\text{afterslip}}$ . The excellent  
 229 agreement between the analytical approach and the numerical simulations is demon-  
 230 strated in Figure 4.

231 We can determine the bound on the slow front scaling relation by noting that  
 232 for infinitesimal  $\bar{\tau}$ ,  $\bar{v}_{c,\infty} \approx 0$  and  $\bar{M}_{0,1D} \approx \frac{\bar{L}^2}{2}$ . This yields

$$\bar{T}_{\bar{\tau}=0} = \bar{v}_{c,0}(1 - \beta)^{\frac{1}{1-\beta}} \bar{L}^{\frac{1}{1-\beta}} + \log(100) \frac{2\bar{L}^2 \bar{\alpha}}{\pi^2}, \quad (19)$$

233 where the first term will dominate over the second term (negligible afterslip) for large  
 234  $\bar{L}$  because  $\frac{1}{1-\beta} > 2$  for the measured  $\beta = 0.6852$ . We can then solve for

$$\bar{L} \approx \frac{\bar{T}_{\bar{\tau}=0}^{1-\beta}}{(1 - \beta) \bar{v}_{c,0}^{1-\beta}} \quad (20)$$

235 which gives us

$$\bar{M}_{0,\text{slow},1D,\bar{\tau}=0} \approx \frac{\bar{L}^2}{2} \propto \bar{T}^{2(1-\beta)} \quad (21)$$

236 with  $2(1 - \beta) \approx 0.6296$ . We also observe a transition to a different scaling at large  
 237  $\bar{M}_{0,1D}$  when  $\bar{\tau}$  is nonzero. To obtain the exponent in this regime, we note that in this  
 238 limit the steady state rupture velocity is reached, so that

$$\bar{T} \approx \frac{\bar{L}}{\bar{v}_{c,\infty}} + \log(100) \frac{2\bar{L}^2 \bar{\alpha}}{\pi^2}. \quad (22)$$

239 For large  $\bar{L}$  and nonzero  $\bar{\tau}$ , the afterslip will dominate, so that  $\bar{L} \propto \bar{T}^{\frac{1}{2}}$ . The cubic  
 240 term in equation 8 will eventually dominate, which results in

$$\bar{M}_{0,\text{slow},1D,\bar{L} \gg 1, \bar{\tau} > 0} \propto \bar{T}^{\frac{3}{2}} \quad (23)$$

241 This means that the moment duration scaling relation in the slow regime is expected  
 242 to follow a power law with exponent  $2(1 - \beta)$  with a possible transition to  $\frac{3}{2}$  at large  
 243  $\bar{M}_{0,1D}$

## 244 4 Discussion

245 We have demonstrated that a simple Burridge-Knopoff model with Amontons-  
 246 Coulomb friction is capable of reproducing the range of power law scaling relations  
 247 between seismic moment and duration observed in nature. The simplicity of the model  
 248 means that we can calculate the scaling relations analytically, and we find the one-  
 249 dimensional exponents  $2(1 - \beta)$  with a transition to  $\frac{3}{2}$  for large seismic moments for  
 250 slow rupture, 2 for sub-shear rupture, and 3 for super-shear rupture, where  $\beta$  is the  
 251 power law exponent of the transient slow rupture velocity.

252 In this letter, we aimed to address two questions. First, whether there is a sep-  
 253 aration of two distinct classes, or is there a continuum of possible scaling relations  
 254 between the fast and slow end-members. We argue that the most likely value for  $\bar{\tau}$  is  
 255 close to 0, which corresponds to shear stress at the dynamic level, or to ruptures where  
 256 the stress drop is small compared to the background stress like in faults (Shearer et  
 257 al., 2006). If this is indeed the case, the moment duration scaling should contain a  
 258 continuum of slip modes between the slow and fast end-members. However, because  
 259 large  $\bar{\tau}$  would in this case be unlikely, it would result in a distinction of fast and slow

260 scalings simply because this is more likely. This would indicate that both the interpre-  
 261 tations by Ide et al. (2007) and by Peng and Gomberg (2010) hold in the sense that  
 262 there is a continuum of slip modes, but the natural variation of  $\bar{\tau}$  could result in more  
 263 frequent events along the end-member scalings.

264 In our simulations, the separation into the slow and sub-shear scaling relations  
 265 occurs spontaneously under the assumption that  $\bar{\tau} \approx 0$ . It has also been suggested that  
 266 the observed separation could be strongly affected by instrumental limitations (Agnew,  
 267 2009). In particular because the vastly different time-scales involved in aseismic and  
 268 sub-shear rupture require different measurement techniques (Gomberg et al., 2016;  
 269 Peng & Gomberg, 2010).

270 The second question we aimed to address was whether a difference in  $M_0 - T$   
 271 scaling relations alone could be attributed to different physical mechanisms behind  
 272 slow and fast rupture. Our model contains only two dimensionless parameters, which  
 273 highlights that the observed scaling relations do not necessitate complex underlying  
 274 mechanisms. The same friction law with different values for the coefficients and a  
 275 varying prestress can explain the entire range of scaling relations, and the slow scaling  
 276 regime arises simply because slow rupture speeds are transient. Our findings thus  
 277 suggest that there could be a separation in slow and fast scalings without a difference  
 278 in physical mechanism. To assign different physical mechanisms to slow and fast  
 279 rupture thus requires more observations than a different scaling relation alone.

280 To compare our results to observations on faults, it is instructive to discuss  
 281 relations that would be obtained for rupture on a 2D plane. If we can assume radial  
 282 symmetry, we can use the same expression for  $\langle \bar{u} \rangle$  as in 1D, but  $\bar{M}_{0,2D} = \langle \bar{u} \rangle \bar{L}^2$ , which  
 283 changes the scaling by a term  $\bar{L}$ . This changes the scaling relations to

$$\bar{M}_{0,\text{sub-shear},2D} \propto \bar{T}^3 \quad (24)$$

$$\bar{M}_{0,\text{super-shear},2D} \propto \bar{T}^4 \quad (25)$$

$$\bar{M}_{0,\text{slow},2D} \propto \bar{T}^{\{3(1-\beta),2\}} \quad (26)$$

286 where  $3(1 - \beta) \approx 0.9444$  is the exponent that is dominant for  $\bar{\tau} = 0$  at large  $\bar{L}$ . This is  
 287 remarkably close to the hypothesized exponent of 1 from observations (Ide et al., 2007).  
 288 The transition from  $3(1 - \beta)$  to 2 also indicates that a simple linear scaling relation  
 289 between seismic moment and duration for slow events is not appropriate, because it is  
 290 only valid at  $\bar{\tau} = 0$ . We find it likely that a scaling in the approximate range  $M_0 \propto T$   
 291 to  $T^2$  should be observed for slow events, depending also on the decaying exponent  
 292  $\beta$ . For a constant  $\bar{\alpha}$ , this variation in the power law exponent occurs due to changes  
 293 in the stress state of the interface. This is in line with observations, where different  
 294 studies have reported on scaling exponents ranging from approximately 1 to 2 (Aguiar  
 295 et al., 2009; Frank et al., 2018; Gao et al., 2012; Ide et al., 2007, 2008).

296 From our results in Figure 3 we are in a position to explain the observed relation  
 297 between average rupture speed and seismic moment (Gao et al., 2012). A transient  
 298 rupture speed with a decaying exponent  $\beta$  would result in a two-dimensional scaling  
 299 relation  $\langle \bar{v}_c \rangle \propto \bar{M}_0^{-\frac{\beta}{3(1-\beta)}}$ . Gao et al. (2012) observed that slow events follow the  
 300 approximate relation  $\langle \bar{v}_c \rangle \propto \bar{M}_0^{-0.5 \pm 0.05}$ , which indicates that  $\beta \approx 0.6 \pm 0.025$ . Using  
 301 equation 26 yields a moment duration scaling relation for slow rupture following  $\bar{M}_0 \propto$   
 302  $\bar{T}^{\{1.1,1.3\}}$ , which is fully consistent with their observed linear relationship between  
 303 seismic moment and duration.

304 Here, we have assumed that propagation is not bounded. Gomberg et al. (2016)  
 305 demonstrated that there will be a change from a two-dimensional scaling to a one-  
 306 dimensional scaling when the rupture propagation goes from unbounded to bounded in  
 307 one of the directions. While we have demonstrated that different scalings can originate  
 308 without such effect, a bounded system would add a number of possible transitions in

309 moment duration, and would in principle allow for scaling relations following both the  
 310 two-dimensional and the one-dimensional exponents.

## 311 5 Conclusion

312 Linear elasticity and Amontons-Coulomb friction with a viscous term is sufficient  
 313 to produce a large variety in scaling exponents between seismic moment and duration.  
 314 This suggests that different scaling relations for fast and slow slip events do not require  
 315 different or complex underlying physical mechanisms. Our findings also suggest that  
 316 there exists a continuum of slip modes between the slow and fast slip end-members,  
 317 but that the natural selection of stress on faults can cause less frequent events in  
 318 the intermediate range. We find that the sub-shear scaling follows  $M_0 \propto T^2$  (which  
 319 corresponds to  $T^3$  in 2D), while the slow scaling follows  $T^{2(1-\beta)}$  (which corresponds to  
 320  $T^{3(1-\beta)}$  in 2D) with a transition to  $T^{\frac{3}{2}}$  ( $T^2$  in 2D) for larger seismic moments depending  
 321 on the prestress.  $\beta \approx 0.6852$  corresponds to the power law decay in the slow rupture  
 322 velocity with time. The model also predicts a separate scaling for super-shear rupture  
 323 with  $M_0 \propto T^3$  ( $T^4$  in 2D).

## 324 Acknowledgements

325 We thank David Morgan, Agnès Helmstetter, Michel Bouchon and Yehuda Ben-  
 326 Zion for providing useful suggestions. K.T acknowledges support from EarthFlows -  
 327 A strategic research initiative by The Faculty of Mathematics and Natural Sciences  
 328 at the University of Oslo. H.A.S acknowledges support from the Research Council of  
 329 Norway through the FRINATEK program, grant number 231621. Code to generate  
 330 the data used for the figures in the manuscript is available on Github (Thøgersen,  
 331 2019).

## 332 References

- 333 Agnew, D. (2009). Instrumental, theoretical, temporal, and statistical challenges in  
 334 the search for transient deformations. In *Agu fall meeting abstracts*.
- 335 Aguiar, A. C., Melbourne, T. I., & Scrivner, C. W. (2009). Moment release rate  
 336 of cascadia tremor constrained by gps. *Journal of Geophysical Research: Solid  
 337 Earth*, 114(B7).
- 338 Amundsen, D. S., Trømborg, J. K., Thøgersen, K., Katzav, E., Malthé-Sørensen,  
 339 A., & Scheibert, J. (2015). Steady-state propagation speed of rupture fronts  
 340 along one-dimensional frictional interfaces. *Physical Review E*, 92(3), 032406.
- 341 Bar-Sinai, Y., Spatschek, R., Brener, E. A., & Bouchbinder, E. (2014). On the  
 342 velocity-strengthening behavior of dry friction. *Journal of Geophysical Re-  
 343 search: Solid Earth*, 119(3), 1738–1748.
- 344 Ben-Zion, Y. (2012). Episodic tremor and slip on a frictional interface with criti-  
 345 cal zero weakening in elastic solid. *Geophysical Journal International*, 189(2),  
 346 1159–1168.
- 347 Bürgmann, R. (2018). The geophysics, geology and mechanics of slow fault slip.  
 348 *Earth and Planetary Science Letters*, 495, 112–134.
- 349 Burridge, R., & Knopoff, L. (1967). Model and theoretical seismicity. *Bulletin of the  
 350 seismological society of america*, 57(3), 341–371.
- 351 Colella, H. V., Dieterich, J. H., & Richards-Dinger, K. B. (2011). Multi-event simu-  
 352 lations of slow slip events for a cascadia-like subduction zone. *Geophysical Re-  
 353 search Letters*, 38(16).
- 354 Frank, W. B., Rousset, B., Lasserre, C., & Campillo, M. (2018). Revealing the clus-  
 355 ter of slow transients behind a large slow slip event. *Science advances*, 4(5),  
 356 eaat0661.
- 357 Gao, H., Schmidt, D. A., & Weldon, R. J. (2012). Scaling relationships of source pa-

- 358 parameters for slow slip events. *Bulletin of the Seismological Society of America*,  
 359 *102*(1), 352–360.
- 360 Gelinck, E., & Schipper, D. J. (2000). Calculation of stribeck curves for line con-  
 361 tacts. *Tribology International*, *33*(3-4), 175–181.
- 362 Gomberg, J., Wech, A., Creager, K., Obara, K., & Agnew, D. (2016). Reconsidering  
 363 earthquake scaling. *Geophysical Research Letters*, *43*(12), 6243–6251.
- 364 Ide, S. (2008). A brownian walk model for slow earthquakes. *Geophysical Research*  
 365 *Letters*, *35*(17).
- 366 Ide, S., Beroza, G. C., Shelly, D. R., & Uchide, T. (2007). A scaling law for slow  
 367 earthquakes. *Nature*, *447*(7140), 76.
- 368 Ide, S., Imanishi, K., Yoshida, Y., Beroza, G. C., & Shelly, D. R. (2008). Bridging  
 369 the gap between seismically and geodetically detected slow earthquakes. *Geo-*  
 370 *physical Research Letters*, *35*(10).
- 371 Liu, Y. (2014). Source scaling relations and along-strike segmentation of slow slip  
 372 events in a 3-d subduction fault model. *Journal of Geophysical Research: Solid*  
 373 *Earth*, *119*(8), 6512–6533.
- 374 Olsson, H., Åström, K. J., De Wit, C. C., Gäfvert, M., & Lischinsky, P. (1998). Fric-  
 375 tion models and friction compensation. *Eur. J. Control*, *4*(3), 176–195.
- 376 Peng, Z., & Gomberg, J. (2010). An integrated perspective of the continuum be-  
 377 tween earthquakes and slow-slip phenomena. *Nature geoscience*, *3*(9), 599.
- 378 Romanet, P., Bhat, H. S., Jolivet, R., & Madariaga, R. (2018). Fast and slow slip  
 379 events emerge due to fault geometrical complexity. *Geophysical Research Let-*  
 380 *ters*, *45*(10), 4809–4819.
- 381 Shearer, P. M., Prieto, G. A., & Hauksson, E. (2006). Comprehensive analysis of  
 382 earthquake source spectra in southern california. *Journal of Geophysical Re-*  
 383 *search: Solid Earth*, *111*(B6).
- 384 Shibazaki, B., Obara, K., Matsuzawa, T., & Hirose, H. (2012). Modeling of slow slip  
 385 events along the deep subduction zone in the kii peninsula and tokai regions,  
 386 southwest japan. *Journal of Geophysical Research: Solid Earth*, *117*(B6).
- 387 Shimamoto, T. (1986). Transition between frictional slip and ductile flow for halite  
 388 shear zones at room temperature. *Science*, *231*(4739), 711–714.
- 389 Thøgersen, K. (2019). *One-dimensional burridge knopoff model*. [https://github](https://github.com/kjetilthogersen/1dBurridgeKnopoffMatlab)  
 390 [.com/kjetilthogersen/1dBurridgeKnopoffMatlab](https://github.com/kjetilthogersen/1dBurridgeKnopoffMatlab). GitHub.
- 391 Thøgersen, K., Sveinsson, H. A., Amundsen, D. S., Scheibert, J., Malthe-Sørensen,  
 392 A., & Renard, F. (2019). A minimal model for slow, sub-rayleigh, super-  
 393 shear and unsteady rupture propagation along homogeneously loaded frictional  
 394 interfaces. *arXiv:1906.06079*.

# Supporting Information for: The moment duration scaling relation for slow rupture arises from transient rupture speeds

Kjetil Thøgersen<sup>1,2</sup> \*, Henrik Andersen Sveinsson<sup>1,3</sup>, Julien Scheibert<sup>4</sup>,

François Renard<sup>1,2,5</sup>, Anders Malthe-Sørensen<sup>1,3</sup>

<sup>1</sup>Physics of Geological Processes, The NJORD Centre, University of Oslo, Norway

<sup>2</sup>Department of Geosciences, University of Oslo, Norway

<sup>3</sup>Department of Physics, University of Oslo, Norway

<sup>4</sup>University of Lyon, Ecole Centrale de Lyon, ENISE, ENTPE, CNRS, Laboratoire de Tribologie et Dynamique des Systèmes LTDS,

F-69134, Ecully, France

<sup>5</sup>University Grenoble Alpes, University Savoie Mont Blanc, CNRS, IRD, IFSTTAR, ISTERre, 38000 Grenoble, France

July 7, 2019, 10:21pm

## 1. Equations of motion

The equation of motion for the 1-dimensional Burridge-Knopoff model with a viscous term  $\alpha\dot{u}_i$  is

$$m\ddot{u}_i = k(u_{i+1} - u_i) + k(u_{i-1} - u_i) - \alpha\dot{u}_i - f_{f,i} \quad (\text{S1})$$

where  $u$  is the displacement,  $m$  is the mass,  $k$  is the spring constant,  $\alpha$  is the viscosity, the blocks are separated by a distance  $\Delta x$ , and  $f_f$  is the friction force.  $f_f$  obeys Amontons-Coulomb law of friction, where a block  $i$  begins to move when the static friction force  $f_{f,\text{stuck}} = \mu_s p_i$  is reached. When moving, the friction force is  $f_{f,\text{moving}} = \mu_d p_i \dot{u}/|\dot{u}|$ . A block arrests when  $\dot{u}$  changes sign. Now assume that all blocks are initialized with positions  $u_i(0)$ . Any additional movement  $u'_i(t)$  can be described by

$$u_i(t) = u_i(0) + u'_i(t). \quad (\text{S2})$$

Combining equation S1 and S2 yields

$$m\ddot{u}_i = k(u'_{i+1} - u'_i) + k(u'_{i-1} - u'_i) - \alpha\dot{u}'_i - f_{f,i} + \tau_i, \quad (\text{S3})$$

where we have introduced the prestress

$$\tau_i = k(u_{i+1}(0) - 2u_i(0) + u_{i-1}(0)). \quad (\text{S4})$$

---

\*kjetil.thogersen@fys.uio.no



We then define the dimensionless variables  $\bar{u} = \frac{u'}{U}$ ,  $\bar{t} = \frac{t}{T}$  and  $\bar{x} = \frac{x}{X}$  so that

$$\ddot{\bar{u}}_i = \frac{kT^2\Delta x^2}{mX^2} \frac{\bar{u}_{i+1} - 2\bar{u}_i + \bar{u}_{i-1}}{\Delta \bar{x}^2} - \frac{\alpha T}{m} \dot{\bar{u}}_i - \frac{T^2}{mU} (f_{f,i} + \tau_i), \quad (\text{S5})$$

where the derivative is now taken with respect to  $\bar{t}$ . The dimensionless speed of sound in the system is

$$\bar{v}_s = \sqrt{\frac{k}{m}} \frac{T}{X} \Delta x. \quad (\text{S6})$$

We select  $T$  and  $X$  so that the speed of sound in dimensionless units is 1:

$$T = \sqrt{\frac{m}{k}}, \quad U = \frac{\mu_s p_i - \mu_d p_i}{k}, \quad X = \Delta x, \quad (\text{S7})$$

we obtain

$$\ddot{\bar{u}}_i + \frac{-\bar{u}_{i-1} - \bar{u}_{i+1} + 2\bar{u}_i}{\Delta \bar{x}^2} + \bar{\alpha}_i \dot{\bar{u}}_i - \bar{\tau}_i^\pm = 0. \quad (\text{S8})$$

Note that this means that we have implicitly chosen  $\Delta \bar{x} = \Delta x / X = 1$ . The dimensionless viscous and prestress parameters are given by

$$\bar{\alpha}_i = \frac{\alpha_i}{\sqrt{km}}, \quad \bar{\tau}_i^\pm = \frac{\tau_i / p_i \mp \mu_k}{\mu_s - \mu_d}, \quad (\text{S9})$$

respectively, where  $\pm$  corresponds to  $\text{sign}(\dot{\bar{u}}_i)$ . Here, we simulate the propagation along homogeneously prestressed interfaces. The constraint  $p\mu_s \geq \tau$  results in the existence of steady state propagation only when  $\bar{\tau} \in [0, 1]$ .

Next, we set the boundary conditions. Block 1 ruptures when the friction force reaches the static friction threshold. If the system is loaded by a spring with spring constant  $K$  driven at velocity  $v$ , this corresponds to adding a force on block 1, which in dimensionless units becomes  $\bar{F}_{\text{driving}} = 1 - \bar{\tau} + \bar{K}\bar{v}\bar{t}$ , where  $\bar{K} = \frac{Kp}{\mu_s - \mu_d}$ . For soft tangential loading, i.e.  $\frac{\bar{K}\bar{v}}{\bar{t}} \ll 1$ , this boundary condition is reduced to  $u_0 = 1 - \bar{\tau}$ .

To predict rebound effects, we need to account for negative velocities in certain simulations. We put the additional constraint  $\mu_k = \mu_s/2$ , which results in  $\bar{\tau}^- = \bar{\tau}^+ + 2$ . A small portion of the simulations we perform will contain oscillations with negative velocities (far) behind the front tip. These negative velocities do not affect the propagation speed, but the detailed dynamics behind the front will depend on  $\mu_k$ . The rebound when the rupture stops is affected by  $\mu_k$ . Our choice makes sure there is usually only one rebound at the leading edge in the simulations, i.e. no significant rebound at the trailing edge.

In the Burridge-Knopoff model, the elastic modulus is given by  $E = \frac{k\Delta x}{S}$ , where  $S$  is the cross-sectional area in the contact between the blocks. In the manuscript, we measure the seismic moment (along a line)

$$M_0 = E\langle u \rangle L \quad (\text{S10})$$

where  $E$  is the elastic modulus, and  $\langle u \rangle$  is the average displacement on a fault of length  $L$ . The dimensionless zeroth order moment is then

$$\bar{M}_0 = \frac{M_0}{XUE} = \langle \bar{u} \rangle \bar{L}, \quad (\text{S11})$$

or equivalently

$$\bar{M}_0 = \frac{M_0 H}{(\mu_s - \mu_d)\sigma_N \Delta x} \quad (\text{S12})$$

where  $H$  is the system thickness,  $\sigma_N$  is the (effective) normal stress and  $\Delta x$  is the block size. The occurrence of  $\Delta x$  in this expression highlights that for a side driven system,  $\Delta x$  is assigned the physical meaning of a nucleation length.  $\bar{M}_0 = 1$  is then the minimum seismic moment that we can measure.

For certain analytical calculations below we will note that the difference equation S8 is an approximation of 1-dimensional elastodynamics and instead use

$$\ddot{u} = \frac{\partial^2 \bar{u}}{\partial \bar{x}^2} - \bar{\alpha} \dot{u} - \bar{\tau}. \quad (\text{S13})$$

### Total slip assuming no stress at dynamic level after rupture

Assume that a rupture stops at length  $\bar{L}$ , and that all blocks slip until equilibrium is reached. This can be approximated as

$$\frac{\partial^2 \bar{u}}{\partial \bar{x}^2} - \bar{\tau} = 0 \quad (\text{S14})$$

with  $\bar{u}(\bar{L}) = 0$ , and  $\partial \bar{u} / \partial \bar{x}|_{\bar{x}=0} = \bar{\tau} - 1$ . This has the solution

$$\bar{u}(\bar{x}) = -\frac{\bar{\tau} \bar{x}^2}{2} - (1 - \bar{\tau}) \bar{x} + \frac{\bar{\tau} \bar{L}^2}{2} + (1 - \bar{\tau}) \bar{L}. \quad (\text{S15})$$

The average slip is then

$$\langle \bar{u} \rangle = \frac{\bar{\tau} \bar{L}^2}{3} + \frac{(1 - \bar{\tau}) \bar{L}}{2}. \quad (\text{S16})$$

### Initial rupture velocity in the slow regime

To obtain a result for the slow front transient scaling, it is useful to calculate the initial velocity: The time it takes from the rupture of block 1 until block 2 ruptures. The boundary conditions are  $\bar{u}_0 = 1 - \bar{\tau} + \bar{u}_1$  and  $\bar{u}_2 = 0$ , which results in

$$\ddot{u}_1 + \bar{\alpha} \dot{u}_1 + \bar{u}_1 - 1 = 0 \quad (\text{S17})$$

This has the solution

$$\bar{u}_1(\bar{t}) = c_1 e^{\frac{1}{2}(-\sqrt{\bar{\alpha}^2 - 4} - \bar{\alpha})\bar{t}} + c_2 e^{\frac{1}{2}(\sqrt{\bar{\alpha}^2 - 4} - \bar{\alpha})\bar{t}} + 1 \quad (\text{S18})$$

Let's start with the overdamped case  $\bar{\alpha} \geq 2$ . The initial conditions are  $\bar{u}_1(0) = \dot{\bar{u}}_1 = 0$ .

$\bar{u}_1(0) = 0$  leads to

$$c_1 + c_2 = -1 \quad (\text{S19})$$

Using also  $\dot{\bar{u}}_1(0) = 0$  leads to

$$c_1 = -\frac{1}{2} \frac{\sqrt{\bar{\alpha}^2 - 4} - \bar{\alpha}}{\sqrt{\bar{\alpha}^2 - 4}} \quad (\text{S20})$$

$$c_2 = \frac{1}{2} \frac{\sqrt{\bar{\alpha}^2 - 4} - \bar{\alpha}}{\sqrt{\bar{\alpha}^2 - 4}} - 1. \quad (\text{S21})$$

We are now looking for the time  $\bar{t}_c$  when  $\bar{u}(\bar{t}_c) = 1 - \bar{\tau}$ .

$$c_1 e^{\frac{1}{2}(-\sqrt{\bar{\alpha}^2 - 4} - \bar{\alpha})\bar{t}_c} + c_2 e^{\frac{1}{2}(\sqrt{\bar{\alpha}^2 - 4} - \bar{\alpha})\bar{t}_c} + 1 = 1 - \bar{\tau} \quad (\text{S22})$$

$$c_1 e^{\frac{1}{2}(-\sqrt{\bar{\alpha}^2 - 4} - \bar{\alpha})\bar{t}_c} + c_2 e^{\frac{1}{2}(\sqrt{\bar{\alpha}^2 - 4} - \bar{\alpha})\bar{t}_c} = -\bar{\tau} \quad (\text{S23})$$

These equations do not have an analytical solution, so we need to make some assumptions to proceed further. The slow slip regime occurs for large  $\bar{\alpha}$ , and since  $\bar{\tau}$  is small, the propagation is slow, and we also expect  $\bar{t}_c$  to be large. In such case, we can assume

$$c_1 e^{\frac{1}{2}(-\sqrt{\bar{\alpha}^2 - 4} - \bar{\alpha})\bar{t}_c} \approx 0, \quad (\text{S24})$$

and instead solve

$$c_2 e^{\frac{1}{2}(\sqrt{\bar{\alpha}^2 - 4} - \bar{\alpha})\bar{t}_c} \approx -\bar{\tau} \quad (\text{S25})$$

which leads to

$$\bar{t}_c \approx \frac{2 \log \left( -\frac{\bar{\tau}}{\frac{1}{2} \frac{\sqrt{\bar{\alpha}^2 - 4} - \bar{\alpha}}{\sqrt{\bar{\alpha}^2 - 4}} - 1} \right)}{\sqrt{\bar{\alpha}^2 - 4} - \bar{\alpha}} \quad (\text{S26})$$

The initial front velocity is found from the inverse and reads

$$\bar{v}_{c,0} \approx \bar{t}_c^{-1} = \frac{\sqrt{\bar{\alpha}^2 - 4} - \bar{\alpha}}{2 \log \left( -\frac{\bar{\tau}}{\frac{1}{2} \frac{\sqrt{\bar{\alpha}^2 - 4} - \bar{\alpha}}{\sqrt{\bar{\alpha}^2 - 4}} - 1} \right)}. \quad (\text{S27})$$

We observe slow slip also in slightly underdamped systems at low  $\bar{\tau}$ , so we need to solve this for the underdamped case as well. Assuming  $\bar{\alpha} < 2$ , we can rewrite the solution of  $\bar{u}_1(\bar{t})$ :

$$\bar{u}_1(\bar{t}) = \left[ -\frac{\bar{\alpha}}{\sqrt{4 - \bar{\alpha}^2}} \sin \left( \frac{\sqrt{4 - \bar{\alpha}^2}}{2} \bar{t} \right) - \cos \left( \frac{\sqrt{4 - \bar{\alpha}^2}}{2} \bar{t} \right) \right] e^{-\frac{\bar{\alpha}}{2} \bar{t}} + 1 \quad (\text{S28})$$

where we have assumed  $\bar{u}(0) = \dot{\bar{u}}(0) = 0$ . Again we look for the time  $\bar{t}_c$  when  $\bar{u}(\bar{t}_c) = 1 - \bar{\tau}$

$$\begin{aligned} & \frac{\bar{\alpha}}{\sqrt{4 - \bar{\alpha}^2}} \sin \left( \frac{\sqrt{4 - \bar{\alpha}^2}}{2} \bar{t}_c \right) \\ & + \cos \left( \frac{\sqrt{4 - \bar{\alpha}^2}}{2} \bar{t}_c \right) = \bar{\tau} e^{\frac{\bar{\alpha}}{2} \bar{t}_c}, \end{aligned} \quad (\text{S29})$$

and again, this equation does not have an analytical solution. We make the additional assumption that  $\bar{t}_c$  is small so that  $\bar{\tau} e^{\frac{\bar{\alpha}}{2} \bar{t}_c} \approx \bar{\tau}$  and solve

$$\frac{\bar{\alpha}}{\sqrt{4 - \bar{\alpha}^2}} \sin \left( \frac{\sqrt{4 - \bar{\alpha}^2}}{2} \bar{t}_c \right) + \cos \left( \frac{\sqrt{4 - \bar{\alpha}^2}}{2} \bar{t}_c \right) \approx \bar{\tau}. \quad (\text{S30})$$

This has the (first) solution

$$\bar{t}_c \approx -\frac{4 \tan^{-1} \left( \frac{\sqrt{-(\bar{\alpha}^2 - 4)((\bar{\alpha}^2 - 4)\bar{\tau}^2 + 4) + \sqrt{4 - \bar{\alpha}^2} \bar{\alpha}}{(\bar{\alpha}^2 - 4)(\bar{\tau} + 1)} \right)}{\sqrt{4 - \bar{\alpha}^2}}. \quad (\text{S31})$$

We can then summarize the results:

$$\bar{v}_{c,0} \approx \begin{cases} -\frac{\sqrt{4 - \bar{\alpha}^2}}{4 \tan^{-1} \left( \frac{\sqrt{-(\bar{\alpha}^2 - 4)((\bar{\alpha}^2 - 4)\bar{\tau}^2 + 4) + \sqrt{4 - \bar{\alpha}^2} \bar{\alpha}}{(\bar{\alpha}^2 - 4)(\bar{\tau} + 1)} \right)}, & \bar{\alpha} < 2 \\ \frac{\sqrt{\bar{\alpha}^2 - 4} - \bar{\alpha}}{2 \log \left( -\frac{\bar{\tau}}{\frac{1}{2} \frac{\sqrt{\bar{\alpha}^2 - 4} - \bar{\alpha}}{\sqrt{\bar{\alpha}^2 - 4}} - 1} \right)}, & \bar{\alpha} > 2 \end{cases} \quad (\text{S32})$$

where we have assumed that  $\bar{\tau}$  is small. Note that the solution is not accurate in the region around  $\bar{\alpha} = 2$ . However, the analytical solution is fairly accurate already at  $\bar{\alpha} \simeq 2.1$ , which we made use of in the main text.

### Afterslip in the slow front regime - Analytical predictions

To be able to make a complete prediction for the seismic moment versus duration, we also need to account for the afterslip. Here, we explore the following question: What is the seismic moment if we exclude afterslip? To obtain this value we cannot use equation 7 but instead may use equation S13

### Afterslip duration in the slow front regime

We make the following assumption: After the front arrests, the shape of the slip profile adapts towards the solution for  $\dot{u} = 0$ . In the following, we have set  $\bar{t} = 0$  to the time when the front arrests. Using the fundamental theorem of analysis we can write

$$\frac{\partial^2 \bar{u}(\bar{x}, \bar{t})}{\partial \bar{x}^2} = \frac{\partial^2 \bar{u}(\bar{x}, \bar{t})}{\partial \bar{x}^2} \Big|_{\bar{t}=0} + \int_0^{\bar{t}} \frac{\partial^2 \dot{\bar{u}}(\bar{x}, \bar{t}')}{\partial \bar{x}^2} d\bar{t}' \quad (\text{S33})$$

Next, we make the assumption that the velocity profile after the front arrests is separable

$$\dot{\bar{u}}(\bar{x}, \bar{t}) = \bar{A}(\bar{t}) \dot{\bar{u}}_0(\bar{x}). \quad (\text{S34})$$

Inserting for  $\dot{\bar{u}}(\bar{x}, \bar{t})$  in equation S33 and combining it with equation S13 yields

$$0 = \frac{\partial^2 \bar{u}(\bar{x}, \bar{t})}{\partial \bar{x}^2} \Big|_{\bar{t}=0} + \int_0^{\bar{t}} \bar{A}(\bar{t}') \frac{\partial^2 \dot{\bar{u}}_0(\bar{x})}{\partial \bar{x}^2} d\bar{t}' - \bar{\alpha} \bar{A}(\bar{t}) \dot{\bar{u}}_0(\bar{x}) + \bar{\tau}, \quad (\text{S35})$$

where we have assumed that accelerations are small ( $\frac{\partial^2 \dot{\bar{u}}_0}{\partial \bar{t}'^2} = 0$ ). We can now take the derivative with respect to  $\bar{t}$  to obtain

$$\frac{\partial}{\partial \bar{t}} \left( \frac{\partial^2 \bar{u}(\bar{x}, \bar{t})}{\partial \bar{x}^2} \right) \Big|_{\bar{t}=0} + \bar{A}(\bar{t}) \frac{\partial^2 \dot{\bar{u}}_0(\bar{x})}{\partial \bar{x}^2} = \bar{\alpha} \dot{\bar{u}}_0(\bar{x}) \frac{\partial \bar{A}(\bar{t})}{\partial \bar{t}} \quad (\text{S36})$$

which can be rewritten as

$$\bar{A}(\bar{0}) \frac{\partial^2 \dot{u}_0(\bar{x})}{\partial \bar{x}^2} + \bar{A}(\bar{t}) \frac{\partial^2 \dot{u}_0(\bar{x})}{\partial \bar{x}^2} = \bar{\alpha} \dot{u}_0(\bar{x}) \frac{\partial \bar{A}(\bar{t})}{\partial \bar{t}} \quad (\text{S37})$$

This should be valid for any choice of  $\bar{x}$  and  $\bar{t}$ . To proceed, we find the relation between  $\dot{u}_0$  and  $\frac{\partial^2 \dot{u}_0}{\partial \bar{x}^2}$  at  $\bar{t} = 0$ .

$$2 \frac{\partial^2 \dot{u}_0(\bar{x})}{\partial \bar{x}^2} \bar{A}(0) = \bar{\alpha} \dot{u}_0(\bar{x}) \frac{\partial \bar{A}(\bar{t})}{\partial \bar{t}} \Big|_{\bar{t}=0} \quad (\text{S38})$$

Next, we insert the general solution  $A(\bar{t}) = e^{-C\bar{t}}$  so that

$$\frac{\partial^2 \dot{u}_0(\bar{x})}{\partial \bar{x}^2} = -\frac{\bar{\alpha} C}{2} \dot{u}_0(\bar{x}) \quad (\text{S39})$$

This has the solution

$$\dot{u}_0(\bar{x}) = c_1 \sin\left(\sqrt{\frac{\bar{\alpha} C}{2}} \bar{x}\right) + c_2 \cos\left(\sqrt{\frac{\bar{\alpha} C}{2}} \bar{x}\right) \quad (\text{S40})$$

The boundary conditions are  $\dot{u}_0(0) = \bar{\tau}/\bar{\alpha}$  (from steady state slip velocity) and  $\dot{u}_0(\bar{L}) = 0$ , which gives

$$c_2 = \frac{\bar{\tau}}{\bar{\alpha}} \quad (\text{S41})$$

and

$$c_1 = -\frac{\bar{\tau}}{\bar{\alpha} \tan\left(\sqrt{\frac{\bar{\alpha} C}{2}} \bar{L}\right)} \quad (\text{S42})$$

resulting in

$$\dot{u}_0(\bar{x}) = \frac{\bar{\tau}}{\bar{\alpha}} \left( \cos\left(\sqrt{\frac{\bar{\alpha} C}{1-C}} \bar{x}\right) - \frac{\sin\left(\sqrt{\frac{\bar{\alpha} C}{1-C}} \bar{x}\right)}{\tan\left(\sqrt{\frac{\bar{\alpha} C}{1-C}} \bar{L}\right)} \right) \quad (\text{S43})$$

We can determine the decay constant  $C$  by using the boundary condition due to soft tangential loading, which is equivalent to

$$\frac{\partial \dot{u}_0(\bar{x})}{\partial \bar{x}} \Big|_{\bar{x}=0} = 0, \quad (\text{S44})$$

which leads to

$$C = \frac{\pi^2}{2\bar{\alpha}\bar{L}^2}. \quad (\text{S45})$$

We can then write out the full expression for the afterslip as a function of  $\bar{x}$  and  $\bar{t}$

$$\dot{\bar{u}}(\bar{x}, \bar{t}) = \frac{\bar{\tau}}{\bar{\alpha}} \left( \cos\left(\sqrt{\frac{\pi^2}{4\bar{L}^2}}\bar{x}\right) - \frac{\sin\left(\sqrt{\frac{\pi^2}{4\bar{L}^2}}\bar{x}\right)}{\tan\left(\sqrt{\frac{\pi^2}{4\bar{L}^2}}\bar{L}\right)} \right) e^{-\frac{\pi^2}{2\bar{\alpha}\bar{L}^2}\bar{t}} \quad (\text{S46})$$

For this to be used to find the afterslip contribution to the seismic moment, we need to calculate  $\langle \bar{u} \rangle(\bar{t})$ .

$$\begin{aligned} \langle \bar{u} \rangle(\bar{t}) &= \frac{1}{\bar{L}} \int_0^{\bar{L}} \int_0^{\bar{t}} \dot{\bar{u}}(\bar{x}, \bar{t}') d\bar{t}' d\bar{x} \\ &= \frac{4\bar{\tau}\bar{L}^2}{\pi^2} \left( 1 - e^{-\frac{\pi^2\bar{t}}{2\bar{\alpha}\bar{L}^2}} \right) \end{aligned} \quad (\text{S47})$$

The characteristic time scale for this decay is

$$\bar{t}_{\text{c,afterslip}} = \frac{2\bar{\alpha}\bar{L}^2}{\pi^2} \quad (\text{S48})$$

The time it takes to accumulate 99% of the afterslip (which we use in the measurements) is then

$$\bar{t}_{\text{afterslip}} = \log(100) \frac{2\bar{\alpha}\bar{L}^2}{\pi^2} \quad (\text{S49})$$

The total amount of afterslip is

$$\langle \bar{u} \rangle_{\text{afterslip}} = \frac{4\bar{\tau}\bar{L}^2}{\pi^2}. \quad (\text{S50})$$

Note that the calculation in this section slightly underestimates the amount of afterslip and the afterslip time because we do not account for the time it takes to reach the steady state velocity profile.